

Single-, Dual- and Wide-Band Frequency-Reconfigurable Antenna with Annular Ring Slots

M. C. Lim¹, S. K. A. Rahim¹, M. R. Hamid², P. J. Soh³, M. I. Sabran¹, A. A. Eteng⁴,
and M. R. Ramli¹

¹Wireless Communication Centre (WCC)
Universiti Teknologi Malaysia, 81310, Johor Bharu, Johor, Malaysia
archuan@gmail.com, sharulkamal@fke.utm.my, mursyid@fkegraduate.utm.my, mrridduan2@live.utm.my

²Radio Communications Engineering
Universiti Teknologi Malaysia, 81310, Johor Bharu, Johor, Malaysia
rijal@fke.utm.my

³Advanced Communication Engineering (ACE) CoE, School of Computer and Communication Eng.
Universiti Malaysia Perlis (UniMAP), Kampus Pauh Putra, 02600 Arau, Perlis, Malaysia
pjsoh@unimap.edu.my

⁴Department of Electronic and Computer Engineering, Faculty of Engineering
University of Port Harcourt, Port Harcourt, Nigeria
akaa.eteng@uniport.edu.ng

Abstract — This paper presents a frequency reconfigurable antenna enabled using a pair of annular ring slots on a coplanar waveguide (CPW) ground plane. Its initial wideband operation mode from 3 GHz to 6 GHz can be reconfigured into six additional modes: a dual-band mode and five single-band modes, with minimum reflection coefficients (S_{11}) of -10 dB. For demonstration and proof-of-concept purposes, metal switches have been used to represent the switches in simulations and measurements. The ON state is emulated using shorted metal switches, whereas the OFF state is emulated using an open. Good agreements are indicated for simulated and measured S_{11} and radiation patterns.

Index Terms — Frequency reconfigurable antenna, CPW, narrowband, wideband.

I. INTRODUCTION

In the past few decades, wireless communication systems are becoming an essential component of daily human life. An important component of such wireless systems is the antenna, which is required to be multi- or wideband. This feature enables hardware efficiency as access to multiple operating frequency band will be enabled using a single antenna. Besides that, the problems of limited spectrum, regulatory and licensing issues are currently being addressed by the use of cognitive radios (CR). In a CR network, the intelligent radio allows unlicensed users (secondary users) to

access spectrum bands licensed to primary users, while avoiding interference with them [1].

To facilitate this, the frequency reconfigurable antenna as it is arguably the most practical option of switching its operation to the desired frequency, instead of utilizing a number of antennas operating in different frequencies for signal transmission or reception. Besides improved performance, multi-frequency operation in a single antenna reduces space and cost. Typically, frequency-reconfigurable antennas can be generally enabled using three methods: mechanical actuation, tuning of material properties and integrating electronic components such as switches or diodes [2]. The third method of using PIN diodes is considered the most practical technique for switching antenna operation between different frequencies [3], [4].

Various previous literature have employed metal switches in proving their concept of reconfiguration. These switches emulate practical microwave switches with realistic amounts of losses. For instance, a frequency reconfigurable tapered slot Vivaldi antenna capable of switching between wideband and narrowband modes using metal switches to control current flow was presented in [5, 6, and 7]. The presence of a metal switch emulates the ON state of a practical microwave switch, whereas its absence emulates the OFF state. Meanwhile, the antenna in [5] uses five ring slots for switching between its wideband mode (from 1.5 GHz to 5 GHz) and another four different sub-bands. Besides

that, four pair of ring slots were implemented in the ground plane to generate a wideband mode (from 2 GHz to 8 GHz), and reconfiguration to other three lower, middle and upper sub-bands [6]. Next, a Vivaldi antenna with defected ground plane formed using a pair of rectangular ring slot was proposed in [7]. This antenna can be operated in three modes: a wideband mode (from 2.2 GHz to 7.2 GHz), a dual-band WLAN mode (from 2.4 GHz to 2.485 GHz and 5.725 GHz to 5.875 GHz) and a single band WLAN mode (from 2.4 GHz to 2.485 GHz). The rectangular slot functions as a stopband filter for resonance induced by the ring slots.

In this letter, a frequency reconfigurable antenna with capability to reconfigure between wideband and dual-band modes is proposed. The dual-band reconfigurability for this antenna is enabled using a similar concept used for the single-band reconfigurability in [4] and [8]. Besides featuring a compact size of $0.502\lambda_0 \times 0.513\lambda_0 \times 0.023\lambda_0$ at 4.3 GHz, it is capable of switching to six sub-bands with the incorporation of a pair of simple ring slot. This proposed antenna features a wideband mode from 3 GHz to 6 GHz, a dual-band operation centered at 3.7 GHz and 5.8 GHz; and five single-band modes resonant at 4.2 GHz, 4.58 GHz, 4.86 GHz, 5.7 GHz and 6 GHz.

II. ANTENNA DESIGN

An elliptical monopole has been selected as the main radiator based on [9], with annular rings implemented on the ground plane for wideband and narrowband re-configurability. The proposed antenna is designed, simulated and optimized using the commercial electromagnetic solver CST Microwave Studio (MWS), which is based on the Finite Integration Technique (FIT). The structure is meshed using 157,500 hexahedral-shaped mesh cells before being solved numerically using the time domain solver in CST. The boundaries of the structure are set to be open, with additional $\lambda/4$ space in all directions based on the lowest simulated frequency. The structure was excited using a 50 Ω port waveguide port. A FR4 substrate, with a relative permittivity (ϵ_r) of 4.7 and loss tangent ($\tan \delta$) of 0.019 is used to ensure a cost-effective implementation. Figure 1 shows the geometry of the proposed antenna operating in its wideband mode (from 3 GHz to 6 GHz in State 1) and dual band mode (centered at 3.7 GHz and 5.8 GHz in State 2) with a S_{11} of -10 dB. Switches are implemented to connect the end points of the rectangular slot, namely S_1 (in State 1) and S_2 (in State 2) in Fig. 1. Table 1 shows the optimized dimensions of the proposed antenna.

To reconfigure resonance, regions with dense surface current distributions are altered by the incorporation of a pair of annular ring slot resonators onto the ground plane. Figure 2 demonstrates its operation in terms of electrical field distribution with and without slot resonator at 3.5 GHz. It is observed

that highly dense electrical fields are distributed along the left resonator slot, whereas this intensity is lower on the right ground plane without the resonator slot. A pair of shorting stub placed on the slot circumference as a RF switch effectively alters the current distribution, resulting in resonance at different frequencies [4], [8]. These switch locations also activate the bandpass function of the antenna, determining the suppressed frequencies, and consequently producing operation in the seven bands.

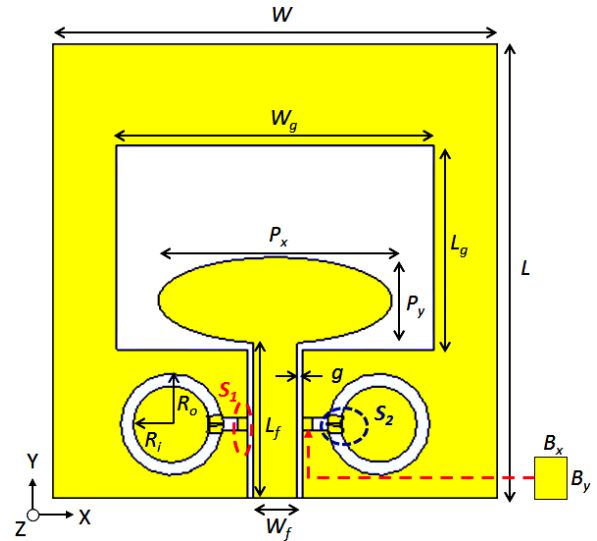


Fig. 1. Geometry of proposed antenna.

Table 1: Parameters of the proposed antenna

Parameter	Dimension [mm]
Width of substrate, W	35
Length of substrate, L	35.8
Gap, g	0.4
Width of CPW ground, W_g	25
Length of CPW ground, L_g	16.11
Width of patch, P_x	18.4
Length of Patch, P_y	6.8
Fed line width, W_f	3.5
Fed line length, L_f	12.2
Ring slot outer radius, R_o	4
Ring slot inner radius, R_i	3
Length of bridge on x, B_x	0.8
Length of bridge on y, B_y	1

The use of either one or two metal switches on each annular ring slot enables reconfigurability between a wide band, a dual band and the five single band modes. They are placed on the two symmetrical ring slots each etched onto the left and the right side of the CPW ground-plane. These switches are placed onto the ring slots with specific clockwise and anti-clockwise rotations, see Fig. 3. The resonator functionality will be

disabled when these switches (S_i) are connected to the ground plane.

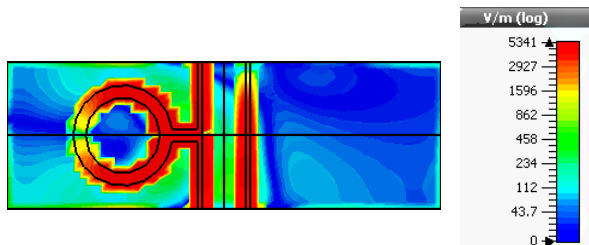


Fig. 2. Simulated E-field distribution.

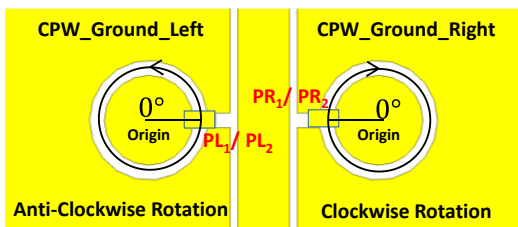


Fig. 3. Geometry of the annular ring slots.

Figure 4 depicts the simulated reflection coefficients for State 1 and State 2. The S_{11} of -13 dB at 4.4 GHz for the State 1 degraded to -4 dB for State 2 upon the shorting of the S_2 annular ring circumference, as illustrated in Fig. 1. This indicates that the ring configuration for the State 2 now functions as a filter. Figures 5 (a) and 5 (b) illustrate the electrical field distributions for the wideband (State 1) and dual-band modes (State 2) at 4.4 GHz. A moderate current density is observed on the ground plane in the wideband mode (State 1). There is a strong current distribution along the perimeter of the resonator in the dual-band mode (State 2), as shown Fig. 5 (b). This length is approximately a quarter-wavelength ($\lambda/4$) at 3.7 GHz.

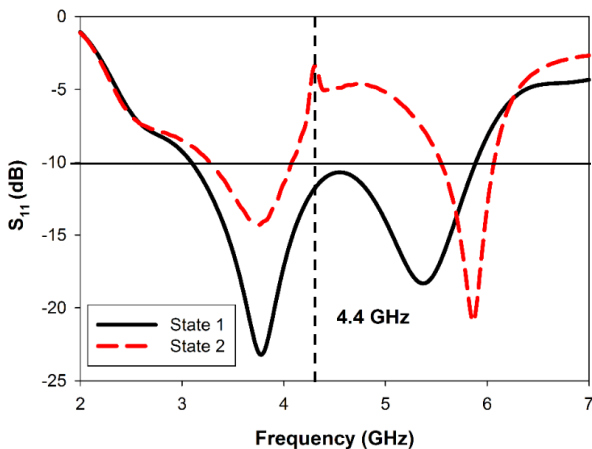


Fig. 4. Simulated reflection coefficients for States 1 and 2.

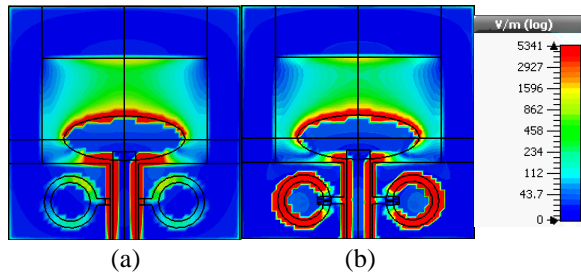


Fig. 5. Simulated E-field distribution at 4.4 GHz for: (a) State 1, and (b) State 2.

To activate the narrowband behavior, the metal switches located at point S_1 need to be disconnected to eliminate wideband mode. The operation of the narrowband states are similar, and is explained by taking State 6 as an example. The simulated S_{11} and S_{21} for this state presented in Fig. 6 indicates a tuned filter behavior, with a pass band at 5.48 GHz located between two stop bands at 2.9 GHz and 6.9 GHz. Placing a shorting stub on each ring slot reduces the electrical field density and isolate both stop bands. The second shorting stub in each slot is used to control the electrical length.

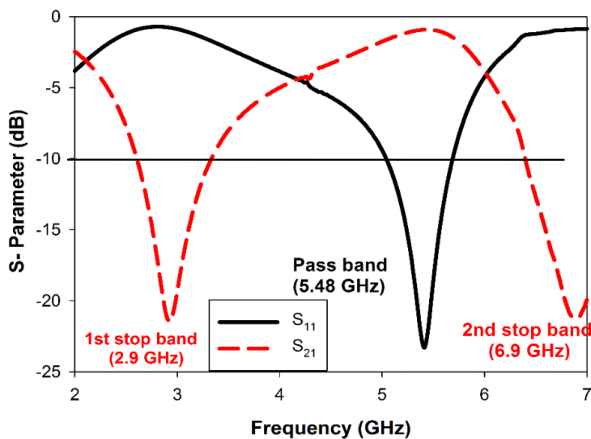


Fig. 6. Simulated S-parameters for State 6.

Figure 7 (a) exhibits the electrical field distribution for the first stop band, with strong electrical fields at 2.9 GHz concentrated in the section S_L (with a length of 14.1 mm). On the other hand, the fields for the second stop band at 6.9 GHz mostly exist within section S_S (with a length of 5.1 mm), as shown in Fig. 7 (b). Both of them are separated by a distance of approximately one sixth of a wavelength in a waveguide ($\lambda_g/6$) at 5.48 GHz in section S_I (with a length of 3.56 mm). The E-Field of the pass band at 5.48 GHz is shown in Fig. 7 (c), indicating high densities in the slot section S_P (with a length of 20.2 mm). The length of this section is approximately equivalent to λ_g at 5.48 GHz. From Fig.

6, the pass band centered at 5.48 GHz is slightly shifted compared to the pass band of State 6 which resonated at 5.7 GHz. This shift is due to the effect of mutual coupling between the patch elements [10]. To further tune the operation of the narrowband modes, locations of these metal switches can be tuned to adjust its electrical length.

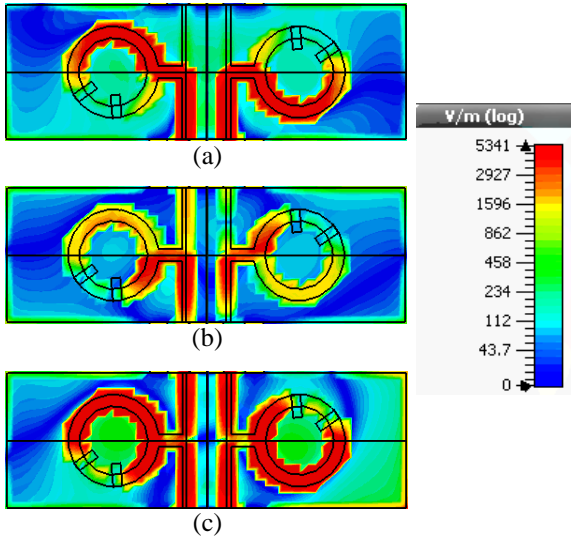


Fig. 7. Simulated E-field distribution of state 6 at: (a) 2.9 GHz, (b) 6.9 GHz, and (c) 5.48 GHz.

III. RESULTS AND DISCUSSION

The proposed antenna has been fabricated to validate its actual antenna performance as seen in Fig. 8. Simulated and measured S_{11} of States 1 (wideband mode) and 2 (dual-band mode) are shown in Fig. 9. The wideband mode is produced by combining and overlapping two resonances at 3.7 GHz and 5.3 GHz [11], resulting in a wider impedance bandwidth. Meanwhile, the dual-band mode is generated by positioning the metal switches in State 2 as listed in Table 2.

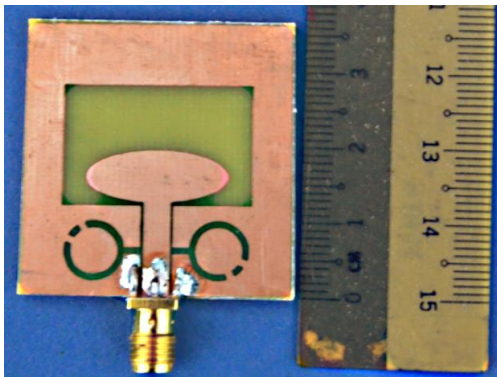


Fig. 8. Photograph of the fabricated antenna (with switch configuration in State 5).

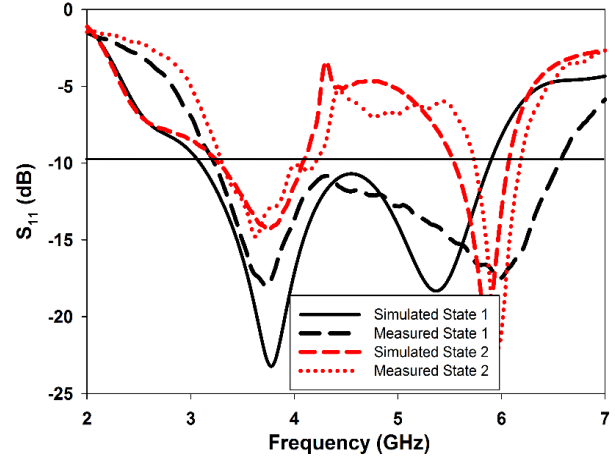


Fig. 9. Simulated vs. measured reflection coefficient for the wideband mode (State 1) and dual-band mode (State 2).

Table 2: Optimal positions of the switches on the annular ring for different states

State #	CPW Ground Left		CPW Ground Right	
	PL ₁	PL ₂	PR ₁	PR ₂
S ₂	5°	355°	5°	355°
S ₃	215°	Nil	215°	Nil
S ₄	115°	135°	215°	145°
S ₅	115°	155°	205°	245°
S ₆	215°	275°	85°	145°
S ₇	195°	275°	85°	165°

Figure 10 shows the simulated and measured S_{11} for the five single band modes centered at 4.2 GHz (State 3), 4.58 GHz (State 4), 4.86 GHz (State 5), 5.7 GHz (State 6) and 6 GHz (State 7). The metal switch configuration for States 2 to 7 are summarized in Table 2. Simulated and measured S_{11} for States 3, 4, 5 and 7 as shown in Fig. 10. There exist small discrepancies between the simulated and measured bandwidths. Besides fabrication inaccuracies caused by the small switch dimensions, there is small disagreements between the material properties (ϵ_r and $\tan \delta$) defined in the simulations compared to its actual value. These properties are defined as constants based on the datasheet provided by the manufacturer in simulations, whereas in practice, their variation may be considerable, especially when the antenna is operated throughout a wide frequency band.

Table 3 summarizes the simulated and measured gain and efficiency obtained at resonance when the proposed antenna is operating in the wideband mode. It indicates that the simulated gain of the wideband mode is between 3.6 dBi and 4.17 dBi, whereas its measured gain is between 3.7 dBi and 4.52 dBi within the 3.7 GHz to 6 GHz operating range. Gains for the narrowband mode presented in Table 4 indicate similarity with gain obtained in the wideband mode. For instance, the gain

at 3.7 GHz for State 1 is 3.76 dBi and State 2 is 3.71 dBi, indicating a discrepancy of only 0.06 dBi. One of the key reasons for this is that there exist no parasitic effects originating from components typically used in the DC biasing circuit. The simulated total efficiency of proposed antenna is between 0.81 and 0.98 for the wideband mode, and between 0.93 and 0.98 for the six narrowband modes. All simulated and measured bandwidths are summarized in Table 5.

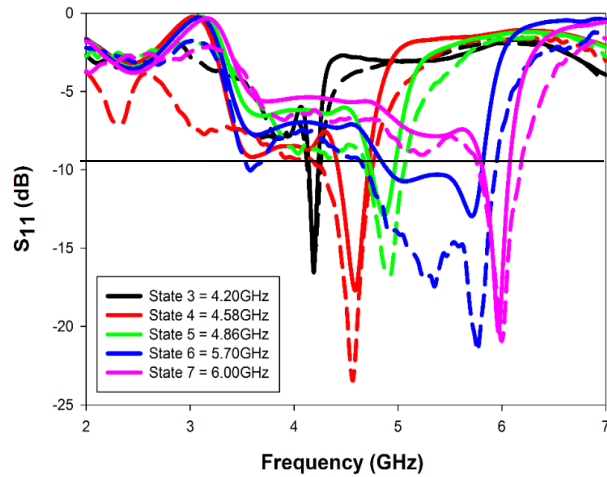


Fig. 10. Simulated (solid line) and measured (dotted line) reflection coefficients (S_{11}) for the single band mode: at 4.2 GHz (State 3), at 4.58 GHz (State 4), at 4.86 GHz (State 5), at 5.7 GHz (State 6), and at 6 GHz (State 7).

Table 3: Gain and total efficiency for the wideband mode
Wideband Mode (State1)

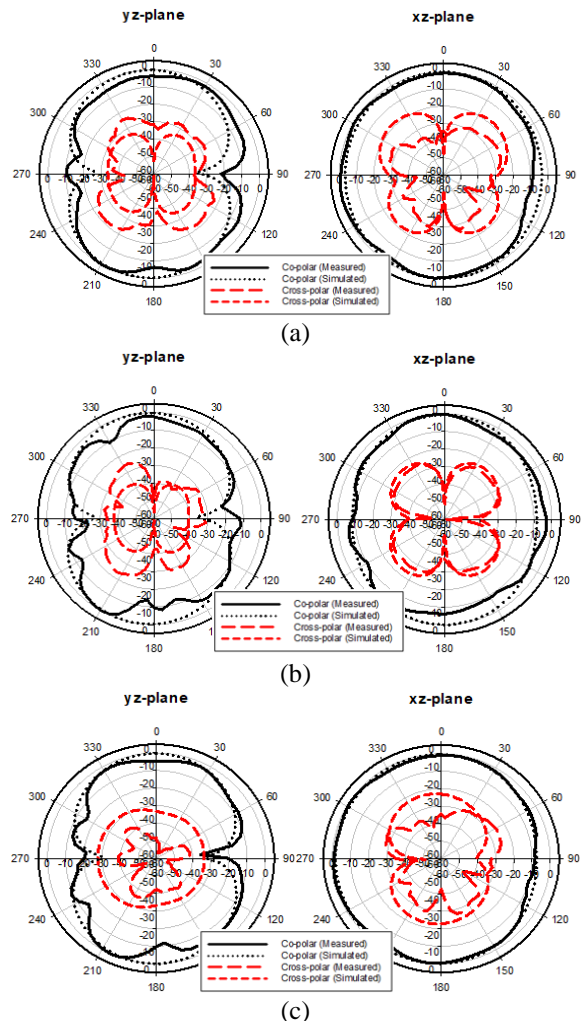
Frequency band (GHz)	3.7	4.2	4.58	4.86	5.7	5.8	6
Simulated gain (dBi)	3.76	4.16	4.12	3.39	3.6	3.8	4.17
Measured gain (dBi)	3.74	4.43	4.52	4.01	3.7	4.08	4.09
Total efficiency (Simulate)	0.98	0.94	0.93	0.97	0.93	0.9	0.81

Table 4: Gain and total efficiency for the narrowband modes

State	2	3	4	5	6	2	7
Frequency band (GHz)	3.7	4.2	4.58	4.86	5.7	5.8	6
Simulated gain (dBi)	3.7	3.54	3.8	3.63	4.07	4.15	4.07
Measured gain (dBi)	3.06	3.82	2.2	3.29	2.27	3.52	3.87
Total efficiency (Simulated)	0.98	0.96	0.96	0.93	0.94	0.98	0.98

Table 5: Summary of the simulated and measured bandwidths for different modes of the proposed reconfigurable antenna

State	Mode	Bandwidth (Simulated)	Bandwidth (Measured)
1	Wideband	3.07-5.92 GHz (63%)	3.22-6.6 GHz (68%)
2	Dual band	3.2-4.06 GHz (24%)	3.32-4.2 GHz (23%)
		5.51-6.05 GHz (5%)	5.53-6.04 GHz (9%)
3	Single band	4.13-4.23 GHz (2%)	4.12-4.24 GHz (3%)
4	Single band	4.42-4.72 GHz (7%)	4.29-4.74 GHz (10%)
5	Single band	4.77-4.98 GHz (4%)	4.7-5.04 GHz (7%)
6	Single band	4.89-5.8 GHz (17%)	4.7-5.93 GHz (23%)
7	Single band	5.81-6.06 GHz (4%)	5.77-6.18 GHz (7%)



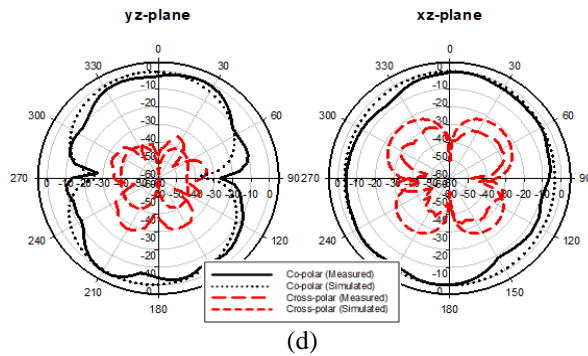


Fig. 11. Simulated and measured radiation patterns in the: (a) wideband mode: State 1 (at 4.5 GHz), (b) dual-band mode: State 2 (at 3.7 GHz), (c) dual-band mode: State 2 (at 5.8 GHz), and (d) single-band mode: State 4 (at 4.58 GHz).

Figures 11 (a) to 11 (d) illustrate the simulated and measured radiation pattern of proposed antenna measured in an anechoic chamber. The radiation pattern for the wideband mode at 4.5 GHz is plotted in Fig. 11 (a), and for the dual-band mode at 3.7 GHz and 5.8 GHz in Figs. 11 (b) and 11 (c). Finally, the single band radiation patterns at 4.58 GHz for State 4 is illustrated in Fig. 11 (d). As can be seen, all co-polarized patterns in the yz-plane exhibit the conventional monopole characteristic which is bi-directional. Meanwhile, the co-polarized xz-plane fields are quasi-omnidirectional. Good agreements between simulated and measured patterns are observed for the proposed antenna.

IV. CONCLUSION

A compact, 35 mm × 35.8 mm CPW-fed frequency reconfigurable antenna capable of switching between wideband, dual-band and narrowband modes is presented. This is enabled via the proper positioning of switches on a pair of slots etched on the ground plane. These resonators act as bandpass filters to suppress unwanted frequencies. The wideband mode is enabled when the metal stubs are located at the edge of ground plane. Meanwhile, one or two metal stubs are located on the annular ring slot to produce narrowband modes. Finally, the dual-band mode is generated by positioning the two switches (S_2) at the center of the rectangular slot connected to the annular ring resonator. Such features are beneficial for frequency switching in cognitive radios and suited for various wireless applications.

REFERENCES

[1] M. Al-Husseini, L. Safatly, A. Ramadan, A. El-Hajj, K. Y. Kaban, and C. G. Christodoulou, "Reconfigurable filter antennas for pulse adaption in UWB cognitive radio systems," *Progress In Electromagnetics Research B*, vol. 37, pp. 327-342, 2012.

[2] N. L. Sudhakar Rao, "An overview of tuning techniques for frequency-agile antennas," *IEEE Antennas and Propagation Magazine*, vol. 54, no. 5, pp. 272-226, 2012.

[3] M. I. Lai, T. Y. Wu, J. C. Hsieh, C. H. Wang, and S. K. Jeng, "Design of reconfigurable antennas based on an L-shaped slot and PIN diodes for compact wireless devices," *IET Microwaves, Antennas & Propagation*, vol. 3, p. 47, 2009.

[4] A. Tariq, M. R. Hamid, and H. Ghafouri-Shiraz, "Reconfigurable monopole antennas," *Proceedings of the 5th European Conference on Antennas and Propagation (EUCAP)*, pp. 2160-2164, 2011.

[5] T. L. Yim, S. K. A. Rahim, and R. Dewan, "Reconfigurable wideband and narrowband tapered slot Vivaldi antenna with ring slot pairs," *Journal of Electromagnetic Waves and Applications*, vol. 27, pp. 276-287, 2013.

[6] M. R. Hamid, P. Gardner, P. S. Hall, and F. Ghanem, "Reconfigurable Vivaldi antenna," *Microwave and Optical Technology Letters*, vol. 52, pp. 785-787, 2010.

[7] M. R. Hamid, P. S. Hall, P. Gardner, and F. Ghanem, "Switched WLAN-wideband tapered slot antenna," *Electronics Letters*, vol. 46, p. 23, 2010.

[8] R. Hamid, P. Gardner, P. S. Hall, and F. Ghanem, "Vivaldi antenna with integrated switchable band pass resonator," *IEEE Transactions on Antennas and Propagation*, vol. 59, pp. 4008-4015, 2011.

[9] M. C. Lim, S. K. A. Rahim, M. I. Sabran, and A. A. Eteng, "Monopole Ellipse Antenna for Ultra-Wideband Applications," *Lecture Notes in Electrical Engineering-Springer*, vol. 344, pp. 137-144, 2015.

[10] H. F. Abutarboush, R. Nilavalan, S. W. Cheung, K. M. Nasr, T. Peter, D. Budimir, *et al.*, "A reconfigurable wideband and multiband antenna using dual-patch elements for compact wireless devices," *IEEE Transactions on Antennas and Propagation*, vol. 60, pp. 36-43, 2012.

[11] A. K. Gautam, S. Yadav, and B. K. Kanaujia, "A CPW-fed compact UWB microstrip antenna," *IEEE Antennas and Wireless Propagation Letters*, vol. 12, pp. 151-154, 2013.



Sultan Abdul Halim Mu'adzam Shah (POLIMAS) and

Lim Meng Chuan was born in Kedah, Malaysia in 1983. He is currently pursuing M.Sc. degree in Universiti Teknologi Malaysia (UTM). He received his dip. in Electronic Engineering (Communication) and B.Sc. degree in Electrical Engineering from Politeknik

Universiti Teknologi Malaysia (UTM) in year 2004 and 2012, respectively. Currently, he is Test Engineer in Multinational Company. His research interests include, Ultra-wideband antenna and reconfigurable antenna.



Sharul Kamal Abdul Rahim received his first degree from University of Tennessee, USA majoring in Electrical Engineering, graduating in 1996, M.Sc. in Engineering (Communication Engineering) from Universiti Teknologi Malaysia (UTM) in 2001, and Ph.D. in

Wireless Communication System from University of Birmingham, UK in 2007. Currently, he is an Associate Professor at Wireless Communication Centre, Faculty of Electrical Engineering, UTM. His research interest is Smart Antenna on Communication System.



Mohamad Rijal Hamid received the Ph.D. degree in Electrical Engineering from the University of Birmingham, UK, in 2011. He has been with the Faculty of Electrical Engineering (FKE), UTM, since 2001. His major research interest is reconfigurable antenna design for

multimode wireless applications. Currently he is a Senior Lecturer at Communication Engineering Dept., FKE, UTM.



Ping Jack Soh was born in Sabah, Malaysia. He received the Bachelor and Master degrees in Electrical Engineering (Telecommunication) from Universiti Teknologi Malaysia (UTM) in 2002 and 2005, respectively, and the Ph.D. degree in Electrical Engineering from KU

Leuven, Belgium in 2013. He is currently a Senior Lecturer at the Advanced Communication Engineering (ACE) CoE, School of Computer and Communication Engineering, Universiti Malaysia Perlis (UniMAP). Soh was the recipient of the IEEE Antennas and Propagation Society (AP-S) Doctoral Research Award in 2012, the IEEE Microwave Theory and Techniques Society (MTT-S) Graduate Fellowship for Medical Applications in 2013 and the International Union of Radio Science (URSI) Young Scientist Award in 2015. He was also the second place winner of the IEEE Presidents' Change the World Competition and IEEE MTT-S Video Competition, both in 2013, besides being awarded the Computer Simulation Technology (CST) University Publication Award in 2011 and 2012.



Mursyidul Idzam Sabran was born in Selangor, Malaysia. He obtained his degree in Electrical Engineering (Telecommunication) in 2009 and M.Sc. in Master of Engineering (Electrical) in 2012 from UTM Skudai, Johor Malaysia. He is currently a full-time Ph.D. research student at the Wireless Communication Centre (WCC), Faculty of Electrical Engineering, Universiti Teknologi Malaysia (UTM), Johor, Malaysia.



Akaa A. Eteng obtained the B.Eng. degree in Electrical/Electronic Engineering from the Federal University of Technology Owerri, Nigeria, in 2002, an M.Eng. degree in Electronics and Telecommunications from the University of Port Harcourt, Nigeria in 2008. In 2016, he obtained a PhD in Electrical Engineering from Universiti Teknologi Malaysia. He is currently a lecturer at the University of Port Harcourt, Nigeria.



Muhammad Ridduan Ramli was born in Kuala Terengganu, Malaysia. He obtained his degree in Electrical (Electronic) Engineering in 2015. He is currently a full-time Master by Research Student at the Wireless Communication Centre (WCC), Faculty of Electrical Engineering, Universiti Teknologi Malaysia, Johor, Malaysia.